A Flexible Voltage Control Strategy Based on Stage-division for Microgrids

Yongjun Zhang, *Senior Member*, *IEEE*, Kaidong Lin, Wenyang Deng, *Member*, *IEEE*, Di Zhang, and Dongliang Xiao

***Abstract*—The occurrence of power flow reversal and off-limit of the voltage on common bus becomes more frequent because of the increasing penetration of renewable energy sources (RES) in microgrids. To guarantee the safe and stable operation, adjusting the power output of RES-based inverters to avoid the off-limit voltage is necessary. Considering the apparent power characteristics of inverters, as well as the minimum participation of active power, a voltage control strategy based on stage division to be within the voltage limit is investigated in this paper. In the case of unknown demand and distribution of loads, the proposed control strategy is able to make full use of the apparent power to regulate voltage using simple calculations, while the performance in economical operation is satisfactory. Simulation results prove the effectiveness of the proposed method on the common bus off-limit voltage adjustment.**

***Index Terms*—Off-limit voltage, microgrids, voltage control, inverter, stage division.**

I. Introduction

Affected by reserves, wars and other unpredictable factors, the price and supply of traditional fossil fuels, such as oil and natural gas, are subject to violent fluctuations [1], [2]. This background promotes the increase of the penetration of renewable energy sources (RES) in microgrids (MGs) [3], such as photovoltaics (PVs) and wind turbines. However, the power output fluctuations of RES-based generation are frequent and irregular, and are highly dependent on meteorological conditions such as temperature, solar radiation, and wind velocity [4]. In addition, the demands of load in MGs change in real time, and do not match with the power output fluctuation of RES [5]. As a result, the high penetration of RES in MGs will bring great challenges to their safe and stable operation.

Received: September 13, 2023
Accepted: February 10, 2024
Published Online: May 1, 2024
Wenyang Deng (corresponding author) is with the School of Electric Power, South China University of Technology, Guangzhou 510640, China (e-mail: dwyang@scut.edu.cn).
DOI: 10.23919/PCMP.2023.000137

To minimize the impact on the voltage of the distribution network, the voltage of a microgrid should be kept stable [6]. However, voltage on the common bus in a microgrid is heavily influenced by the status of RES and loads. When the load demand increases and/or the RES-based generation output power is insufficient, the voltage on the common bus may decrease. Conversely, when the load demand is at a lower level and/or the RES output power is high, reverse power flow may occur, causing the voltage at the bus to increase, potentially surpassing the upper limit within the tolerant voltage fluctuation range [7]. These two scenarios of voltage conditions can seriously jeopardize the loads and compromise the safe and stable operation of an MG system. Typically, output active power is usually pulled up from the RES to raise the common bus voltage, and additional reactive power compensation devices, like static var generators (SVGs) or active power filters (APFs), are also applied to achieve this target. Reducing the RES's output of active power has been proven to be an effective solution for restraining the off-limit voltage [8]. Thus, traditional voltage regulation methods usually involve many active power and reactive power compensation devices to keep the voltage stable. However, these solutions are not economic, and the waste of renewable energy is inevitable. In addition, extra equipment for reactive power compensation will increase the total cost of the MG system [9].

To solve the shortcomings of traditional schemes, various solutions have been proposed. In [10], a detailed summary of the characteristics and applications of control methods is provided, based on active power regulation, reactive power regulation, tap changers adjustment, and multi-device coordinative control in low-voltage networks. It is found that under unsatisfied communication conditions, it is difficult to use the coordinative control scheme widely, so over-limit voltage can only be decreased by implementing local control schemes on the nodes. Because of the response time restriction of shunt capacitor-based reactive power compensation equipment, as well as the mechanical wear of traditional transformers with on-load tap changers, it is difficult for the system to respond to the rapid and frequent changes of the RES's output power.

In a low-voltage network with lower resistance and reactance feeders, the inverter of the RES generation can achieve quick and continuous power adjustment. This is more economical and effective than other voltage regulation methods. This conclusion shows the inapplicability of the traditional control scheme under high penetration of renewable energy, and the paper proves the technical feasibility of the inverter-based voltage control method.

Reference [11] proposes an evaluation method and adequacy index of reactive power margin in low voltage networks, when the inverter's apparent power and node voltage offset constraints are met. In addition, the local active/reactive power control strategy is also investigated. However, the calculation process of this method is complex, and is not suitable for engineering implementation. A strategy to handle the off-limit voltage is proposed in [12], in which it reduces or limits the output active power and uses the residual reactive apparent power of the inverter. While this solution is desirable there exists the possibility of wasting renewable energy. Based on voltage sensitivity analyses, reference [13] derives a conversion method between active and reactive power, and realizes the node voltage control without communication. Nevertheless, this method ignores the economic requirements of microgrid systems. An alternative way is proposed in [14] to transform the bi-level programming mathematical model into a single-level programming problem, to calculate the maximum access apparent power of inverter under voltage constraints. However, this method limits the total apparent power of the microgrid.

Researchers have developed many inverter voltage regulation methods based on power electronic control technology. They can be divided into two categories: one is based on control algorithm, and the other is using physical topology. Droop control based on P-F and Q-V curves have been widely used [15]. This method enables adaptive voltage-frequency regulation and automatic power sharing without any communication [16]. Because of the mismatched line impedance of parallel-connected inverters, the voltage regulation performance on the point of common coupling (PCC) bus is affected. Therefore, a current feedback loop-droop control method is proposed to achieve accurate reactive power sharing [17], [18]. The current feedback loop is developed as a virtual impedance loop, and various droop control methods based on that impedance have been studied [19]–[21]. Some are designed to achieve accurate reactive power sharing [19], while others can improve voltage regulation [20], [21].

Physical component-based solutions usually modify the coupling impedance frame, and a typical frame is L-C cascade topology [21]. Benefiting from the series capacitance, the inverter connected to this structure has larger reactive power compensation capacity and stronger voltage regulation ability. Also, reactive power compensation can be performed when the DC voltage is lower than the AC bus voltage with this structure [22].

In summary, most current research on voltage control techniques under high-penetration of renewable energy directly optimize and coordinate the controllable equipment such as tap changers, energy storage units, and reactive power compensation devices, etc. However, there is a lack of studies on a voltage control algorithm considering the apparent power characteristics of an RES-based inverter. In this paper, an inverter voltage control method based on stage division is proposed to solve the problem of off-limit common bus voltage due to high penetration of renewable energy in MGs. Compared with traditional methods, the advantages of the proposed method include:

1) The dependence on grid communication is minimal, reducing the burden of the communication system and avoiding negative effects caused by signal delay.

2) A linear calculation method is applied to the proposed strategy. It is simple in process with a reduced calculation burden.

3) Additional equipment costs can be avoided, promoting economic efficiency and making it more suitable for practical engineering applications.

The whole paper is structured as follows. A voltage control stages analysis is proposed in Section II and the power calculation method is presented in Section III. Sensitivity analysis of inverter voltage control strategies is provided in Section IV, while the proposed voltage control method is described in details in Section V. To prove the effectiveness of the proposed method, a simulation validation is demonstrated in Section VI. At last, a conclusion is offered in Section VII.

II. Stage Analysis of Voltage Control

A. Voltage Regulation Requirements of MGs

For a microgrid system, a common bus may contain several nodes to connected RES-based inverters and loads. The voltage on nodes may be lower than the rated value in the period with low penetration of renewable energy and peak load. In such a scenario, the inverter should generate capacitive reactive power to adjust the power factor, and to raise the voltage. This solution is able to improve the utilization of the inverter's apparent power, the additional reactive power compensation on the feeder can be reduced, while the power loss and voltage drop on the common bus in the MG can be decreased.

When the RES penetration rate is high, the MG will usually experience a node voltage exceeding the upper tolerance limit, while the oversupplied active power injected by the RES generation into feeders is the fundamental factor [13]. At present, the inverter needs to reduce the output active power, to alleviate the harm to the loads and ease the stress on the feeders that is due to the high

voltage. However, this method can cause RES energy waste, affecting the economic operation of the system.

Generally, considering that there is increasing RES access to the MG system, the primary requirement is the off-limit voltage regulation.

B. Analysis of the Working Stages of the Inverter

RES-based inverters perform reactive-voltage control within their power regulation range. Assuming the power factor should not be less than 0.98 (leading or lagging) when the active power output from the inverter is greater than 50% of its rated power, the process of voltage regulation involving the inverter can be divided into 3 stages, as Fig. 1 shows. In addition, Fig. 1 also illustrates RES's active/reactive power changes at different stages, while the range of power factor is within the half circle. Detailed descriptions of stages are provided as following Subsections.

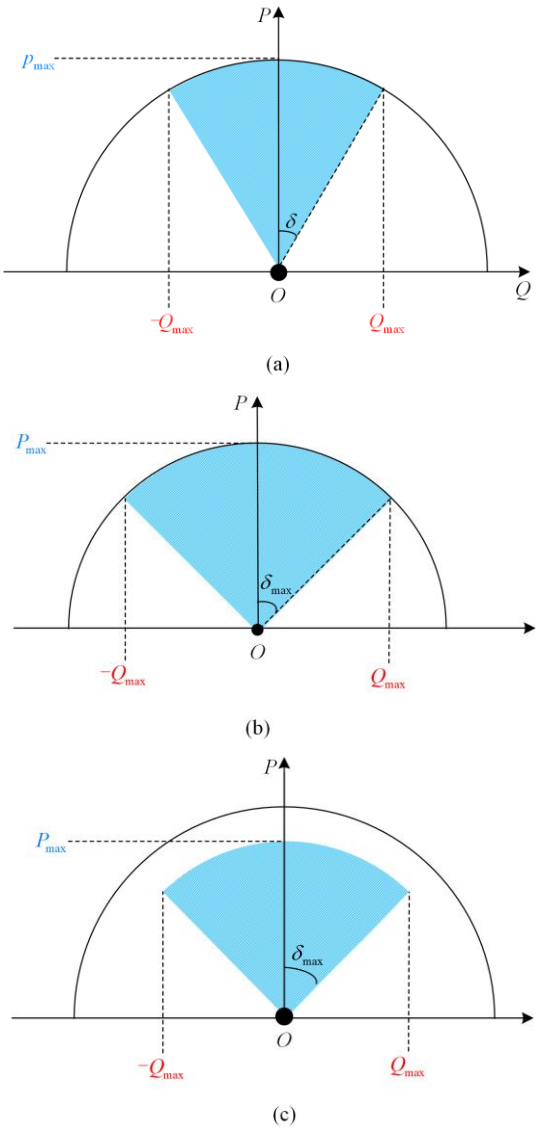

Fig. 1. Inverter output power range in different stages. (a) DRC stage. (b) APL stage. (c) PFL stage.

1) Stage of Dynamic Reactive Power Compensation

In the stage of dynamic reactive power compensation (DRC), the active power of the inverter remains unaffected. As the power angle δ varies, and the output reactive power varies as well. The relationship between the variables in this stage is shown in (1). Elevated reactive power will promote the inverter to reach the maximum power point, and the power angle is noted as the apparent power constraint angle of the inverter.

$$\begin{cases} \cos\delta = \dfrac{P_{out}}{\sqrt{P_{out}^2 + Q_{out}^2}} \\ \delta_{lim} = \arccos\left(\dfrac{P_{out}}{S_{max}}\right) \end{cases} \tag{1}$$

where the output active and reactive power are marked as P_{out} and Q_{out}, respectively; and δ_{lim} presents the power angle restricted by the capacity.

2) Stage of Apparent Power Limitation

In the stage of apparent power limitation (APL), the apparent power S of the inverter remains at the maximum value S_{max}. The reactive power Q_{out} continues to increase with the increase of the power angle δ, while the active power P_{out} decreases. The relationship between the variables at this stage satisfies:

$$\begin{cases} P_{out} = S_{max}\cos\delta \\ Q_{out} = S_{max}\sin\delta \end{cases} \tag{2}$$

3) Stage of Power Factor Limitation

In the stage of power factor limitation (PFL), the inverter is running at the maximum δ_{max}, and the apparent power is reduced to S. The relationship between variables in this stage satisfies:

$$\begin{cases} P_{out} = S\cos\delta_{max} \\ Q_{out} = S\sin\delta_{max} \end{cases} \tag{3}$$

The three stages discussed above described all possible states of the inverter when it is involved in voltage regulation. The values and ranges of the active power, reactive power , apparent power S, and power angle δ of the inverter in the different stages are listed in Table I. It is worth noting that after the DRC, if the power angle has reached before S equals , the apparent power limitation will not appear, i.e., the inverter does not go through all 3 stages when it is in voltage regulation. This is related to the current operating state of the inverter.

TABLE I
RELATIONSHIP BETWEEN THE VARIABLES OF THE INVERTER AT DIFFERENT STAGES

Stage	P_{out}	Q_{out}	S	δ
DRC	P_{out}	$P_{out}\tan\delta$	$P_{out}\sqrt{1+\tan^2\delta}$	0–δ_{max}
APL	$S_{max}\cos\delta$	$S_{max}\sin\delta$	S_{max}	δ_{lim}–δ_{max}
PFL	$S\cos\delta_{max}$	$S\sin\delta_{max}$	0–S_{max}	δ_{max}

C. Control Process Based on Stage Division

Considering the various power angles and capacity restriction of the inverter, the control stages have been presented above. By following the principle of minimizing the active power reduction, the process of the proposed control method is presented in Fig. 2.

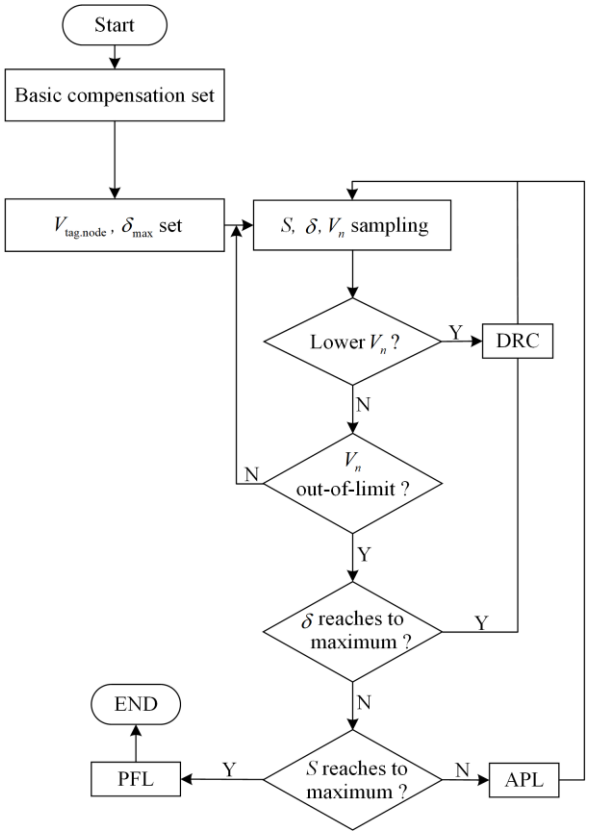

Fig. 2. Control process of the proposed method.

As shown, the tolerant voltage $V_{n,\lim}$ at the common bus and the maximum power angle $\delta_{\max}$ of the inverter are set first, and then, the apparent power *S*, the power angle δ of the inverter, and the node voltage V_n, are sampled and monitored, where the subscript *n* is the number of nodes. If $V_k > V_{k,\lim}$, the apparent power of the inverter *S* has not reached $S_{\max}$, and the power angle δ has not reached the maximum value $\delta_{\max}$. The inverter enters the DRC, i.e., by adjusting the power angle δ of the inverter, it transfers inductive reactive power without reducing its active power. If $V_k > V_{k,\lim}$, the apparent power *S* of the inverter has reached $S_{\max}$, while the power angle δ has not yet reached $\delta_{\max}$, so the inverter enters APL, i.e., it adjusts the power angle δ and transfers more reactive power Q_{out} by reducing the output active power. If $V_k > V_{k,\lim}$, and the power angle δ is equal to $\delta_{\max}$, the inverter enters PFL, i.e., voltage regulation is achieved by reducing the total power of the inverter.

III. Power Calculations of the Inverter-based Voltage Regulation

Assuming the proposed method is applied to an MG system with *n* nodes, as shown in Fig. 3, node 0 on the PCC point is a balancing node. The node *k* is the access point for the RES, and the node voltage amplitude is marked as V_k, while demand of the connected load on this node is $P_k + \mathrm{j}Q_k$. The feeder impedance between node 0 and *k* is $R_{\Sigma k} + \mathrm{j}X_{\Sigma k}$, while the output power of RES-based inverter is $P_{\text{out}} + \mathrm{j}Q_{\text{out}}$. The proposed voltage control strategy uses a linear calculation with fast computation and control response, so that load changes can be considered as small during the voltage adjustment.

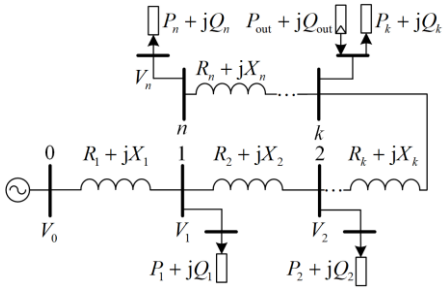

Fig. 3. A typical topology of microgrid with multi-modes.

A. Control in Stage of DRC

When the RES is in normal operation, the inverter usually works at the point of maximum power factor, and the voltage V_k at the access point of RES can be obtained from:

$$V_0 = V_k + \frac{\sum_{i=0}^{k}\left[(\sum_{j=i}^{n} P_j)R_{\Sigma i} + (\sum_{j=i}^{n} Q_j)X_{\Sigma i}\right] - P_{\text{out}}R_{\Sigma k}}{V_k} \tag{4}$$

where V_0 is the voltage on the PCC bus.

At the stage of DRC, the voltage on the access point of RES is adjusted to the target voltage $V_{k,\lim}$ by the reactive power generated from the inverter, given as:

$$V_0 = V_{k,\lim} + \frac{\sum_{i=0}^{k}\left[(\sum_{j=i}^{n} P_j)R_{\Sigma i} + (\sum_{j=i}^{n} Q_j)X_{\Sigma i}\right] - P_{\text{out}}R_{\Sigma k} - Q_{\text{out,b}}X_{\Sigma k}}{V_{k,\lim}} \tag{5}$$

where $Q_{\text{out,b}}$ is the inductive reactive power that is required to reduce the voltage V_k to the target voltage $V_{k,\lim}$. From (4) and (5), there is:

$$Q_{\text{out,b}} = \frac{\boldsymbol{A}}{X_{\Sigma k}} \tag{6}$$

where the term $\boldsymbol{A}$ is:

$$\boldsymbol{A} = V_0(V_k - V_{k,\lim}) + V_{k,\lim}^2 - V_k^2 \tag{7}$$

When the apparent power of the inverter reaches the maximum value $S_{\max}$, if the voltage on the access point still exceeds the limit, the control strategy will enter the APL.

B. Control in Stage of APL

When the inverter reaches the maximum apparent power $S_{\max}$, the power angle of the inverter is $\delta_{\lim}$, while the voltage V_k on the access point is:

$$V_k = V_0 - \frac{\sum_{i=0}^{k}\left((\sum_{j=i}^{n}P_j)R_{\Sigma i} + (\sum_{j=i}^{n}Q_j)X_{\Sigma i}\right)}{V_k} - \frac{S_{\max}(R_{\Sigma k}\cos\delta_{\lim} + X_{\Sigma k}\sin\delta_{\lim})}{V_k} \tag{8}$$

After entering the APL, the apparent power of the inverter always remains at $S_{\max}$. After power angle adjustment, the voltage on the access point is adjusted to the target voltage $V_{k,\lim}$, i.e.:

$$V_{k,\lim} = V_0 - \frac{\sum_{i=0}^{k}\left((\sum_{j=i}^{n}P_j)R_{\Sigma i} + (\sum_{j=i}^{n}Q_j)X_{\Sigma i}\right)}{V_{k,\lim}} - \frac{R_{\Sigma k}P_{\text{out,t}} - X_{\Sigma k}\sqrt{S_{\max}^2 - P_{\text{out,t}}^2}}{V_{k,\lim}} \tag{9}$$

From (7) and (8), the active power from the inverter after the APL, i.e. $P_{\text{out, t}}$, can be obtained as:

$$P_{\text{out,t}} = \frac{(\boldsymbol{A}+\boldsymbol{B})R_{\Sigma k} + \boldsymbol{C}X_{\Sigma k}}{R_{\Sigma k}^2 + X_{\Sigma k}^2} \tag{10}$$

where there are:

$$\begin{cases} \boldsymbol{B} = S_{\max}(R_{\Sigma k}\cos\delta_{\lim} + X_{\Sigma k}\sin\delta_{\lim}) \\ \boldsymbol{C} = \left[(S_{\max}R_{\Sigma k})^2 + (S_{\max}X_{\Sigma k})^2 - (\boldsymbol{A}+\boldsymbol{B})^2\right]^{\frac{1}{2}} \end{cases} \tag{11}$$

C. Control in Stage of PFL

If the off-limit voltage on the access point of the RES cannot be shaved after the above two stages, the output active power from the inverter must be reduced. The reduction is calculated as follows.

When the inverter is operated at the maximum power angle $\delta_{\max}$, the voltage V_k on the access point satisfies:

$$V_0 = V_k + \frac{\sum_{i=0}^{k}(\sum_{j=i}^{n}P_j)R_{\Sigma i} + (\sum_{j=i}^{n}Q_j)X_{\Sigma i}}{V_k} - \frac{S_{\max}\cos\delta_{\max}(R_{\Sigma k} + X_{\Sigma k}\tan\delta_{\max})}{V_k} \tag{12}$$

In the PFL, the power angle of the inverter stays at $\delta_{\max}$. and after power reduction, the voltage on the access point of RES is adjusted to the target voltage $V_{k,\lim}$, and satisfies:

$$V_0 = V_{k,\lim} + \frac{\sum_{i=0}^{k}(\sum_{j=i}^{n}P_j)R_{\Sigma i} + (\sum_{j=i}^{n}Q_j)X_{\Sigma i}}{V_{k,\lim}} - \frac{P_{\text{out,s}}(R_{\Sigma k} + X_{\Sigma k}\tan\delta_{\max})}{V_{k,\lim}} \tag{13}$$

Combining (10) and (11), the output active power of the inverter after the PFL, i.e. $P_{\text{out,s}}$, is:

$$P_{\text{out,s}} = S_{\max}\cos\delta_{\max} + \frac{\boldsymbol{A}}{R_{\Sigma k} + X_{\Sigma k}\tan\delta_{\max}} \tag{14}$$

It can be found from (6), (9) and (12) that the active power P_{out} and the reactive power P_{out} are only related to the common bus voltage V_0, the voltage on access point of RES V_k, and the feeder impedances $R_{\Sigma k}$ and $X_{\Sigma k}$. The real-time and past data of V_k are obtained from the measurement and historical records, the voltage on the common bus V_0 can be obtained by means of communication, and the feeder impedances are obtained by measuring and evaluating the estimated length and type of the feeder.

IV. Sensitivity Analysis of Inverter Voltage Control Strategies

As stated, in the proposed method, V_0, V_k, $R_{\Sigma k}$ and $X_{\Sigma k}$ are the control parameters required for the calculation, while the output active/reactive power are the state variables.

The feeder impedance $R_{\Sigma k}$ and $X_{\Sigma k}$ can be measured and evaluated as presented. Nevertheless, errors are inevitable, while the voltages on the common bus and access point are usually hard to obtain in time because of the potential communication delay. This will lead to inaccuracy in the voltage control, and thus the sensitivity of the proposed strategy to the control parameters (V_0, $R_{\Sigma k}$, and $X_{\Sigma k}$) needs to be analyzed.

A. Sensitivity of the Control Strategy to the Parameters

When there are errors in control parameters, the deviation matrix $\Delta\boldsymbol{V}_k$ of the voltage on the access point of RES caused by the errors can be expressed as:

$$\Delta\boldsymbol{V}_k = \boldsymbol{M}\begin{bmatrix}\Delta R_{\Sigma k} & \Delta X_{\Sigma k} & \Delta V_0\end{bmatrix}^{\mathrm{T}} \tag{15}$$

where $\Delta R_{\Sigma k}$, $\Delta X_{\Sigma k}$, and ΔV_0 are the deviations of control parameters. Matrix $\boldsymbol{M}$ is the sensitivity matrix of the node voltage V_k to the control parameters, given as:

$$\boldsymbol{M} = \begin{bmatrix}\boldsymbol{M}_R^{U_k} \\ \boldsymbol{M}_X^{U_k} \\ \boldsymbol{M}_U^{U_k}\end{bmatrix}^{\mathrm{T}} = \begin{bmatrix}\boldsymbol{M}_Q^{U_k} \\ \boldsymbol{M}_P^{U_k}\end{bmatrix}^{\mathrm{T}}\begin{bmatrix}\boldsymbol{M}_R^{Q} & \boldsymbol{M}_X^{Q} & \boldsymbol{M}_U^{Q} \\ \boldsymbol{M}_R^{P} & \boldsymbol{M}_X^{P} & \boldsymbol{M}_U^{P}\end{bmatrix} \tag{16}$$

where $\boldsymbol{M}_U^{U_k}$, $\boldsymbol{M}_R^{U_k}$, and $\boldsymbol{M}_X^{U_k}$ are the sensitivity matrices of V_k to V_0, feeder parameters $R_{\Sigma k}$ and $X_{\Sigma k}$, respectively; $\boldsymbol{M}_P^{U_k}$ and $\boldsymbol{M}_Q^{U_k}$ are the sensitivity matrices of V_k to P_{out} and Q_{out}, respectively. These can be obtained from the Jacobi matrix in the power flow calculation, whereas the other variables are similar.

B. Power Correction Calculation

In the above discussion, the measurement deviations of the control parameters obtained from the engineering implements, and the horizontal component of the voltage drop are ignored. To realize the accurate adjustment of the voltage, a calculation method for the real-time correction of the output power from the inverter is proposed in this paper. Here, DRC is taken as an example for illustration.

We assume V_k is a function of Q_{out}, which is given by $V_k = f(Q_{\text{out}})$. In order to adjust V_k to be always smaller than the upper limit voltage $V_{k,\text{lim}}$, the actual reactive power to be transferred by the inverter is $Q_{k,\text{out}}$, which is:

$$Q_{k,\text{out}} = Q_{\text{out,b}} + \Delta Q_{\text{out,b}} \tag{17}$$

where $Q_{\text{out,b}}$ is the calculated reactive power in the DRC in (6); and $\Delta Q_{\text{out,b}}$ is the corrected value of reactive power and satisfies:

$$f(Q_{\text{out,b}} + \Delta Q_{\text{out,b}}) = V_{k,\text{lim}} \tag{18}$$

Since the control parameter errors are relatively small compared to the true values, $\Delta Q_{\text{out,b}}$ is also small, so the first-order Taylor series expansion of (17) at $Q_{\text{out,b}}$ is:

$$f(Q_{\text{out,b}}) + \left.\frac{\partial f}{\partial Q}\right|_{Q_{\text{out,b}}} \Delta Q_{\text{out,b}} - V_{k,\text{lim}} = 0 \tag{19}$$

where $f(Q_{\text{out,b}})$ is the voltage after applying (6), and is denoted as $V_{k,\text{b}}$. Since the measurement and calculation errors are small, the voltage and reactive power are considered to be linearly related. Thus, the slope of the V_k-Q_{out} curve at $Q_{\text{out,b}}$ can be approximated as:

$$\left.\frac{\partial f}{\partial Q}\right|_{Q_{\text{out,b}}} = \frac{V_{k,\text{lim}} - f(0)}{Q_{\text{out,b}}} \tag{20}$$

where $f(0)$ is the voltage before reactive power compensation, denoted as $V_{k,0}$. Substituting (18) into (17), the correction of reactive power $\Delta Q_{\text{out,b}}$ can be calculated:

$$\Delta Q_{\text{out,b}} = \frac{V_{k,\text{lim}} - V_{k,\text{b}}}{V_{k,\text{b}} - V_{k,0}} Q_{\text{out,b}} \tag{21}$$

Similarly, assuming the voltage on the access point after applying (9) and (12) are $V_{k,\text{t}}$ and $V_{k,\text{s}}$, respectively, the active power correction values $\Delta P_{\text{out,t}}$ and $\Delta P_{\text{out,s}}$ in the APL and PFL are:

$$\begin{cases} \Delta P_{\text{out,t}} = \dfrac{(V_{k,\text{lim}} - V_{k,\text{t}})(P_{\text{out,t}} - S_{\max}\cos\delta_{\min})}{V_{k,\text{t}} - V_{k,\text{l}}} \\ \Delta P_{\text{out,s}} = \dfrac{(V_{k,\text{lim}} - V_{k,\text{s}})(P_{\text{out,s}} - S_{\max}\cos\delta_{\max})}{V_{k,\text{s}} - V_{k,\text{m}}} \end{cases} \tag{22}$$

where $V_{k,\text{l}}$ and $V_{k,\text{m}}$ are the voltage values at the access point when the inverter is operated at $\delta_{\min}$ and $\delta_{\max}$, respectively.

V. Realization of the Proposed Voltage Control Strategy

The specific implementation steps of the proposed voltage control strategy are:

Step 1: Setting the target limit voltage $V_{k,\text{lim}}$ for the access point of RES and the maximum power angle of the inverter $\delta_{\max}$, as per the local load conditions.

Step 2: Monitoring the apparent power of inverter *S*, power angle δ, and node voltage V_k, and calculating the limit power angle δ_{lim} according to (2).

1) if the node voltage V_k exceeds the limit and the power angle δ is less than δ_{lim}, perform Step 3.

2) if the node voltage V_k is beyond the limit, the inverter has reached the maximum apparent power $S_{\max}$, and the power angle does not meet $\delta_{\max}$, perform Step 4.

3) if the inverter reaches the maximum power angle $\delta_{\max}$, perform Step 5.

4) if the node voltage V_k does not reach the limit, continue with Step 2.

Step 3: Entering the DRC. The reactive power $Q_{\text{out,b}}$ transferred by the inverter is calculated using (6), and is corrected according to (19). Then go to Step 6.

Step 4: Entering the APL. The active power from the inverter $P_{\text{out,b}}$ is obtained using (9), and is corrected according to (20). Then go to Step 6.

Step 5: Entering the PFL. The active power $P_{\text{out,s}}$ from the inverter is calculated using (12), and is corrected according to (21). Then go to Step 6.

Step 6: Output the control signals as per the proposed method, then continue with Step 2.

VI. Simulation Validation

To ensure the effectiveness of the proposed voltage regulation strategy, in this section a case study is presented using the IEEE 33-node model. In the simulation, the interconnection switches are all open, while the three-stage balanced static load model is adopted. The target node voltage limit $V_{\text{lim}} = 1.07$ p.u., and the inverter minimum power angle $\cos(\delta_{\max}) = 0.98$.

A. Analysis of Voltage Control Results in the DRC of the Inverter

Assuming an RES employing PV is connected to node 18 with the active power capacity $P_{\text{PV}} = 2.1$ kW,

the apparent power of the RES-based inverter is $S_{\max} = 2.121$ kVA. The output values of the PV panel are the sampled data of the PV power station in the authors' university on a day in the summer of 2022.

Figure 4(a) shows the variation curve of the per-unit voltage at the access point of the RES, and the inverter's output power during the day under the proposed voltage control strategy. The solid line in Fig. 4(b) is the curve of the active power from inverter changing with the light intensity in the day.

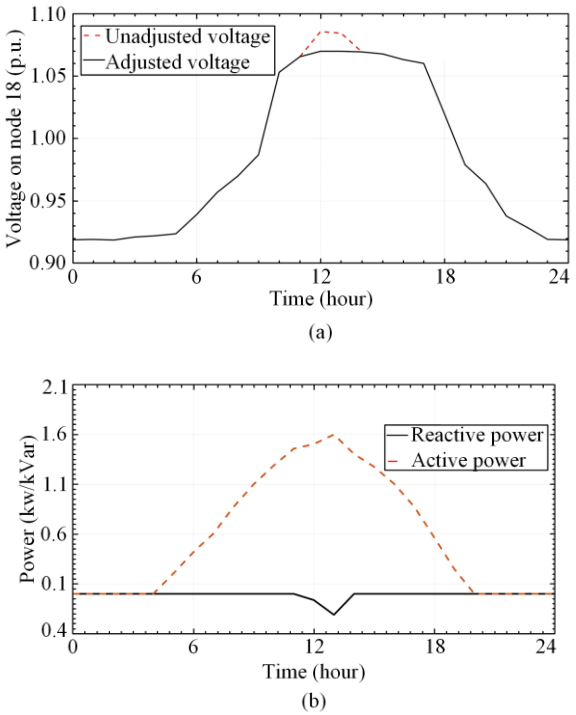

Fig. 4. Voltage and inverter output power curves over the course of a day on Node 18. (a) voltage varies. (b) output power of the inverter.

As can be seen in Fig. 4(a), the voltage at node 18 increases with the increase in active power output from the inverter. If the voltage is not adjusted, the voltage of node 18 will go beyond the limit in the time period of 11:07–14:03. Applying the proposed voltage control strategy, the inverter compensates using its inductive reactive power from 11:07, as stated in the DRC, and the reactive power variation curve is shown in Fig. 4(b). Finally, after the activities in the DRC, the voltage on node 18 is stabilized at $V_{\lim}$.

Figure 5 shows a comparison of the voltage distribution at each node before and after the inverter applies the proposed voltage control strategy at 12:00. As can be seen, the voltage on node 18, i.e. V_{18} is 1.0835 p.u. before the voltage regulation. The calculated results after the implementation of the proposed voltage control strategy are shown in Table II. In the DRC, the inductive reactive power from the inverter $Q_{\text{out}} = 0.2108$ kvar, where the voltage at node 18 is adjusted to 1.0732 p.u., and after the correction as (20), the inductive reactive power from the inverter is adjusted to 0.2597 kvar and the voltage at the access point is stabilized at 1.07 p.u.

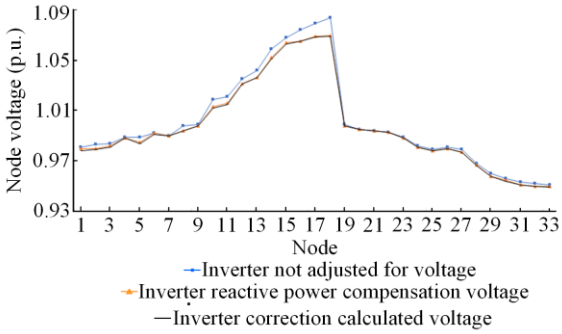

Fig. 5. Comparison of node voltages with different control strategies.

TABLE II
COMPARISON OF RESULTS UNDER DIFFERENT CONTROL STRATEGIES

Voltage control	Amplitude of node voltage V_k	Active power P_{out} (kW)	Reactive power Q_{out} (kvar)	Power factor	Apparent power of inverter (kVA)
Unregulated	1.0835	2.1	0	1	2.1
reactive power compensation	1.0732	2.1	0.2108	0.9950	2.11
Correction calculation	1.0700	2.1	0.2597	0.9925	2.116

B. Analysis of the Effectiveness of the Proposed Voltage Control Strategy

We assume an RES is connected at node 16 with an inverter of maximum apparent power $S_{\max} = 2.121$ kVA. When the output active power $P_{\text{PV}} = 2.1$ kW, the voltage at the access point of the RES is $V_{16} = 1.0898$ p.u.

Figure 6 shows the node voltage distribution during the three different stages. The calculation results of the proposed voltage control strategy are shown in Table III and the calculation procedure is:

1) From the process of the proposed voltage control strategy in Section IV, the first stage is the DRC. As calculated by (7), if the inverter adjusts the node voltage to $V_{\lim}$ by means of reactive power compensation, the required inductive reactive power Q_{out} is 0.7576 kvar. When the inverter reaches maximum power with a power angle of 0.99, the output inductive reactive power Q_{out} is 0.2977 kvar, while V_{16} is 1.0823 p.u. and is still beyond the limit. The voltage control strategy shifts to the APL.

2) In the APL, as calculated by (10), if the voltage at node 16 reaches $V_{\lim}$ by adjusting the apparent power of the inverter, the active power P_{out} should be adjusted to 2.0978 kW. However, when the power angle of the inverter reaches $\delta_{\max}$, the inverter transfers 2.0831 kW of active power and 0.3992 kvar of inductive reactive

power. At this time, $V_{16}=1.0785$ p.u., and the voltage limit is still exceeded. Thus, the voltage control strategy is transferred to the PFL.

3) In the PFL, the output active power P_{out} is reduced to 2.0153 kW as calculated by (13), the voltage on node 16 drops to 1.0715 p.u., and the output active power is then corrected by (22) to a value of $\Delta P=-0.173$ kW. Finally, the inverter transfers 1.9980 kW of active power and 0.4078 kvar of inductive reactive power. The voltage at node 16 is stabilized at 1.07 p.u.

In this case, the inverter goes through three stages and finally achieves accurate control of the voltage at the access point of the RES. It can be seen that the proposed voltage control strategy can effectively solve the problem of node voltage increasing beyond limits caused by high penetration of RES.

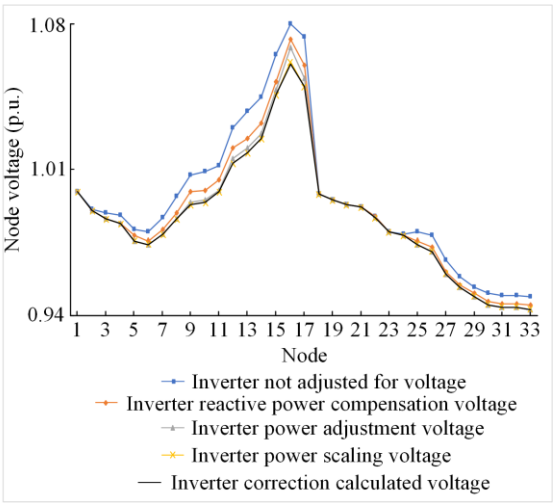

Fig. 6. Comparison of node voltages with different control strategies.

TABLE III
COMPARISON OF RESULTS WITH DIFFERENT CONTROL STRATEGIES

Inverter voltage control	Amplitude of node voltage (V)	*P* (kW)	*Q* (kVar)	PF	Apparent power of inverter (kVA)
Unregulated	1.0898	2.1000	0	1	2.1000
Reactive power compensation	1.0823	2.1000	0.2977	0.99	2.1210
Power adjustment	1.0785	2.0831	0.3992	0.98	2.1210
Power reduction	1.0715	2.0153	0.4120	0.98	2.0570
Correction calculation	1.0700	1.9980	0.4078	0.98	2.0392

C. Error Sensitivity of the Voltage Control Strategy to the Control Parameters

The sensitivity simulation is based on the calculation in Section IV. A. When the relative deviations $\Delta R_{\Sigma 16}/R_{\Sigma 16}=1\%$ for the resistance values of node 0 and node 16, $\Delta R_{\Sigma 16}/R_{\Sigma 16}=1\%$ for the reactance values and $\Delta V_0/V_0=1\%$ for the common bus voltage, the situation will result in a relative error of 4.7% for the active power and 0.59% for the voltage on node 16. The corrected active power from the inverter is 1.9987 kW, the reactive power is 0.3702 kvar, and the voltage on node 16 is stabilized at 1.07 p.u. Table IV shows the voltage variations with the control strategy proposed in this paper in the presence of deviations in the control parameters. It can be seen that in the presence of errors, the proposed control strategy can still achieve accurate voltage control by correcting the calculation.

TABLE IV
COMPARISON OF VOLTAGE CONTROL EFFECTS IN THE PRESENCE OF ERRORS IN THE CONTROL PARAMETERS

Inverter voltage control	Node voltage amplitude	Active power	Reactive power	Power factor	Apparent power of inverter
Unregulated	1.0898	2.1000	0	1	2.1000
Reactive power compensation	1.0823	2.1000	0.2977	0.99	2.1210
Power adjustment	1.0785	2.0831	0.3992	0.98	2.1210
Power reduction	1.0719	2.0162	0.3717	0.98	2.0501
Correction calculation	1.0700	1.9987	0.3702	0.98	2.0320

VII. CONCLUSION

To solve the off-limit voltage problem caused by high-penetration of RES, an inverter-based voltage control strategy is proposed in this paper, and calculation methods of power output adjustment with different voltage control strategies are investigated. Simulation results prove the effectiveness and merits of the proposed method. The main contributions of this paper include:

1) An inverter-based voltage control strategy is proposed. This gives priority to voltage control by adjusting the power angle of inverter, to avoid the reduction of active power as far as possible to ensure maximum power tracking of RES. Only if the node voltage still exceeds the limit when the power angle reaches the maximum, will the output active power be reduced.

2) To adjust the off-limit voltage, the calculation method for the active/reactive power adjustments of the inverter is investigated by considering the topological characteristics of the microgrid, feeder parameters, and the operating stages of the inverter.

3) The sensitivity of the errors in the control parameters to the active/reactive power is analyzed and simulated, and a real-time correction calculation method for the output power is proposed to achieve accurate voltage control.

Compared with the traditional way of regulating voltage by adding reactive power compensation equipment, the solution proposed here makes full use of the apparent power, and the ability to quickly and continuously perform power adjustment of the inverter. This leads to reduced investment in equipment costs, realizes

simple and fast calculation, and is more suitable for practical application.

ACKNOWLEDGMENT

Not applicable.

AUTHORS' CONTRIBUTIONS

Yongjun Zhang: provided supervison of the whole research, and also in charge of project management. Kaidong Lin: analyzed the data and contributed to writing the original draft of the manuscript. Wenyang Deng: constructed the conceptualization and methodology of the proposed novel method, and was responsible for drafting the original manuscript. Di Zhang: performed case studies and validated the rationality of the results. Dongliang Xiao: checked and revised English expression. All authors read and approved the final manuscript

FUNDING

This work is jointly supported by the Guangdong Basic and Applied Basic Research Foundation (No. 2022A1515110794) and the Research and Development Program Project in Key Areas of Guangdong Province (No. 2021B0101230001).

AVAILABILITY OF DATA AND MATERIALS

Please contact the corresponding author for data material request.

DECLARATIONS

Competing interests: The authors declare that they have no known competing financial interests or personal relationships that could have appeared to influence the work reported in this paper.

AUTHORS' INFORMATION

Yongjun Zhang received the Ph.D. degree in power system and its automation from the South China University of Technology, where he is currently a professor. His research interests include power system reactive power optimization, distributed generation control and optimization, voltage control, energy saving, and high-voltage direct current transmission.

Kaidong Lin received M.Sc. degree from Guangdong University of Technology in 2020, and he is now working toward to the Ph.D. degree in the Department of Electric Power, South China University of Technology, Guangzhou, China. His research interests include regulation of MG and AC/DC hybrid power grid.

Wenyang Deng obtained the M.Sc. degree in electrical power system engineering from the University of Manchester, Manchester, U.K., and the Ph. D. degree in electrical computer engineering from the University of Macau. Dr. Deng is now a postdoctoral fellow with the School of Electric Power, South China University of Technology, Guangzhou, China. His research interests include regulation of MG and AC/DC hybrid power grid.

Di Zhang received the Ph.D. degree in electrical engineering from the College of Electrical and Information Engineering, Hunan University, Changsha, China, in 2022. She is currently working as a postdoctoral researcher at the South China University of Technology, Guangzhou, China. Her major research interests include power system operation and control, demand side response, and application of artificial intelligence in power systems.

Dongliang Xiao received the B.S. degree from Harbin University of Science and Technology, Harbin, China, in 2013, the M.S. degree from Harbin Institute of Technology, Harbin, China, in 2015, and the Ph.D. degree from University of Nebraska-Lincoln, Lincoln, USA, in 2019. In 2019, he was a research intern at Mitsubishi Electric Research Laboratories, Cambridge, USA. He is currently a postdoctoral fellow with the Department of Electric Power, South China University of Technology, Guangzhou, China. His research interests include power and energy system optimization, electricity markets and risk management, and renewable energy integration in smart grid.

REFERENCES

[1] W. Wang, S. Huang, and G. Zhang *et al*., "Optimal operation of an integrated electricity-heat energy system considering flexible resources dispatch for renewable integration," *Journal of Modern Power Systems and Clean Energy*, vol. 9, no. 4, pp. 699-710, Jul. 2021.

[2] Y. Yoo, S. Jung, and G. Jang, "Dynamic inertia response support by energy storage system with renewable energy integration substation," *Journal of Modern Power Systems and Clean Energy*, vol. 8, no. 2, pp. 260-266, Mar. 2020.

[3] K. A. Tahir, M. Zamorano, and J. O. García, "Scientific mapping of optimisation applied to microgrids integrated with renewable energy systems," *International Journal of Electrical Power & Energy Systems*, vol. 145, Feb. 2023.

[4] Z. Yang, L. Xia, and X. Guan, "Fluctuation reduction of wind power and sizing of battery energy storage systems in microgrids," *IEEE Transactions on Automation Science and Engineering*, vol. 17, no. 3, pp. 1195-1207, Jul. 2020.

[5] X. Chen, K. C. Leung, and A. Y. S. Lam, "Power output smoothing for renewable energy system: planning, algorithms, and analysis," *IEEE Systems Journal*, vol. 14, no. 1, pp. 1034-1045, Mar. 2020.

[6] Z. Ma, Q. Zhang, and Z. Wang, "Safe and stable secondary voltage control of microgrids based on explicit

neural networks," *IEEE Transactions on Smart Grid*, vol. 14, no. 5, pp. 3375-3387, Sept. 2023.

[7] S. Bera, S. Chakraborty, and S. Kar *et al*, "Hierarchical control for voltage unbalance mitigation considering load management in stand-alone microgrid," *IEEE Transactions on Smart Grid*, vol. 14, no. 4, pp. 2521-2533, Jul. 2023.

[8] W. Deng, N. Dai, and K. W. Lao, "A virtual-impedance droop control for accurate active power control and reactive power sharing using capacitive-coupling inverters," *IEEE Transactions on Industry Applications*, vol. 56, no. 6, pp. 6722-6733, Dec. 2020.

[9] G. S. Lee, D. H. Kwon, and Y. K. Kim *et al.*, "A new communication-free grid frequency and ac voltage control of hybrid LCC-VSC-HVDC systems for offshore wind farm integration," *IEEE Transactions on Power Systems*, vol. 38, no. 2, pp. 1309-1321, Mar. 2023.

[10] R. An, Z. Liu, and J. Liu *et al*., "A comprehensive solution to decentralized coordinative control of distributed generations in islanded microgrid based on dual-frequency-droop," *IEEE Transactions on Power Electronics*, vol. 37, no. 3, pp. 3583-3598, Mar. 2022.

[11] M. Ahmed, R. Bhattarai, and S. J. Hossain *et al*., "Coordinated voltage control strategy for voltage regulators and voltage source converters integrated distribution system," *IEEE Transactions on Industry Applications*, vol. 55, no. 4, pp. 4235-4246, Aug. 2019.

[12] J. Chen, C. Zhang, and P. Yang *et al*., "Off-limit voltage control of high proportion photovoltaic distribution network based on active-reactive power combined regulation," in *the 2nd International Conference on Electronic Materials and Information Engineering*, Hangzhou, China, Apr. 2022, pp. 1-4.

[13] L. Wang, F. Bai, and R. Yan *et al*., "Real-time coordinated voltage control of PV inverters and energy storage for weak networks with high PV penetration," *IEEE Transactions on Power Systems*, vol. 33, no. 3, pp. 3383-3395, May 2018.

[14] M. Y. Y. U. Haque, M. R. Islam, and T. Ahmed *et al*., "Improved voltage tracking of autonomous microgrid technology using a combined resonant controller with lead-lag compensator adopting negative imaginary the orem," *Protection and Control of Modern Power Systems*, vol. 7, no. 1, pp. 1-16, Jan. 2022.

[15] Y. Wang, J. Tang, and J. Si et al., "Power quality enhancement in islanded microgrids via closed-loop adaptive virtual impedance control," Protection and Control of Modern Power Systems, vol. 8, no. 1, pp. 1-17, Jan. 2023.

[16] A. S. Vijay, M. C. Chandorkar, and S. Doolla, "A system emulator for ac microgrid testing," *IEEE Transactions on Industry Applications*, vol. 55, no. 6, pp. 6538-6547, Dec. 2019.

[17] M. Ebrahimi, S. A. Khajehoddin, and M. Karimi-Ghartemani, "An improved damping method for virtual synchronous machines," *IEEE Transactions on Sustainable Energy*, vol. 10, no. 3, pp. 1491-1500, Jul. 2019.

[18] V. Gurugubelli, A. Ghosh, and A. K. Panda, "Parallel inverter control using different conventional control methods and an improved virtual oscillator control method in a standalone microgrid," *Protection and Control of Modern Power Systems*, vol. 7, no. 3, pp. 1-13, Jul. 2022.

[19] V. Gurugubelli, A. Ghosh, and A. K. Panda, "Parallel inverter control using different conventional control methods and an improved virtual oscillator control method in a standalone microgrid," *Protection and Control of Modern Power Systems*, vol. 7, no.1, pp. 1-13, Jul. 2022.

[20] T. K. Roy, S. K. Ghosh, and S. Saha, "Robust backstepping global integral terminal sliding mode controller to enhance dynamic stability of hybrid ac/dc microgrids," *Protection and Control of Modern Power Systems*, vol. 8, no. 1, pp. 1-13, Jan. 2023.

[21] W. Deng, Y. Zhang, and Y. Tang *et al*., "A neural network-based adaptive power-sharing strategy for hybrid frame inverters in a microgrid," *Frontiers in Energy Research*, vol.10, Jan. 2023.

[22] W. Deng, N. Y. Dai, and K. W. Lao *et al*., "An enhanced power decoupling control for grid-connected capacitive-coupling inverters," in *2019 IEEE Energy Conversion Congress and Exposition (ECCE)*, Baltimore, USA, Oct. 2019, pp. 1466-1473.